

# Tri-path DINO: Feature Complementary Learning for Remote Sensing Multi-Class Change Detection

Kai Zheng<sup>1</sup> , Hang-Cheng Dong<sup>1</sup> , Shoulei Liu, Zhenkai Wu , Fupeng Wei , Lei Ding , Wei Zhang\* 

**Abstract**—In remote sensing imagery, multi-class change detection (MCD) is crucial for fine-grained monitoring, yet it has long been constrained by complex scene variations and the scarcity of detailed annotations. To address this, we propose the Tri-path DINO architecture, which adopts a three-path complementary feature learning strategy to facilitate the rapid adaptation of pre-trained foundation models to complex vertical domains. Specifically, we employ the DINOv3 pre-trained model as the backbone feature extraction network to learn coarse-grained features. An auxiliary path also adopts a siamese structure, progressively aggregating intermediate features from the siamese encoder to enhance the learning of fine-grained features. Finally, a multi-scale attention mechanism is introduced to augment the decoder network, where parallel convolutions adaptively capture and enhance contextual information under different receptive fields. The proposed method achieves optimal performance on the MCD task on both the Gaza facility damage assessment dataset (Gaza-change) and the classic SECOND dataset. Grad-CAM visualizations further confirm that the main and auxiliary paths naturally focus on coarse-grained semantic changes and fine-grained structural details, respectively. This synergistic complementarity provides a robust and interpretable solution for advanced change detection tasks, offering a basis for rapid and accurate damage assessment.

**Index Terms**—Change detection, Normalized detector, Change extractor, Mask classification

## I. INTRODUCTION

Remote sensing change detection, which aims to identify regions of interest that have changed between bi-temporal satellite images, plays an irreplaceable role in numerous scenarios such as urban environmental monitoring, agricultural

surveillance, disaster assessment, and damage evaluation [1]. However, Binary Change Detection (BCD) [2] merely answers “where changes have occurred,” offering limited actionable information that is often insufficient to guide follow-up actions. Semantic Change Detection (SCD) [3], on the other hand, requires performing full semantic segmentation on both images before comparing them, which is computationally intensive and demands exhaustive annotation of all semantic categories in both temporal phases. For example, in post-disaster damage assessment, knowing only that “changes have occurred” is far from adequate. It is also essential to clarify “what the changes signify” and to complete the assessment rapidly. Therefore, under real-world constraints, a balance must be struck between efficiency and performance. Multi-class change detection (MCD) [4] addresses this need by subdividing changes into specific semantic categories, thereby providing finer-grained information while significantly reducing annotation effort. This makes MCD a suitable solution for time-sensitive tasks such as rapid damage assessment.

Despite its practical potential, the technical implementation of MCD remains challenging. In real-world scenarios, changed areas are typically small, occupying only a fraction of the total image pixels. Furthermore, due to factors such as damage or degradation, the features distinguishing different change categories are often subtle, making accurate classification particularly difficult. Traditional approaches, including deep learning methods based on siamese networks, commonly suffer from performance degradation due to insufficient information. Additionally, while powerful self-supervised foundation models such as DINOv3 [5] are capable of extracting rich, hierarchical features, they have not yet been fully explored or adapted for this specific task. Direct application often fails to explicitly model and integrate the complementary features needed to distinguish fine-grained inter-class differences within changed regions, such as variations in structural damage severity.

To address the challenges inherent in the MCD task, we propose Tri-path DINO, a novel architecture specifically designed for it. The core innovation of Tri-path DINO is a “third-path” complementary learning strategy, which explicitly extracts and synergizes features at different granularities. The first path serves as the main pathway, utilizing the pre-trained DINOv3 backbone to encode robust, coarse-grained semantic representations. Subsequently, multi-scale intermediate features from the main siamese encoder are progressively aggregated. A Transformer architecture is then employed as an auxiliary siamese encoder to extract fine-grained features. We term this secondary siamese encoder the “third path”, corresponding to

Kai Zheng is with the School of Computer Science and Technology, Zhejiang University, Hangzhou 310027, China (e-mail: zhengkai1990@zju.edu.cn).

Hang-Cheng Dong is with School of Instrumentation Science and Engineering, Harbin Institute of Technology, Harbin 150001, China, and also with Harbin Institute of Technology Suzhou Research Institute, Suzhou 215000, China (e-mail: hunsen\_d@hit.edu.cn)

Liu Shoulei is with Ningbo Haichuang Group Co., Ltd., Ningbo 315300, Zhejiang, China

Zhenkai Wu is with the School of Software Technology, Zhejiang University, Hangzhou 310027, China. (e-mail: xwma@zju.edu.cn)

Fupeng Wei is with School of Information Engineering, North China University of Water Resources and Electric Power, Zhengzhou 450046, China, and also with School of Computer Science, University of Auckland, Auckland, New Zealand

Lei Ding is with the Department of Geo-spatial Information, Information Engineering University, Zhengzhou 450001, China

Wei Zhang is with the School of Software Technology, Zhejiang University, Hangzhou 310027, China, and also with the Innovation Center of Yangtze River Delta, Zhejiang University, Jiaxing, Zhejiang 314103, China (e-mail: estzhangwei@zju.edu.cn).

<sup>1</sup>Kai Zheng and Hang-Cheng Dong contribute equally.

\*Corresponding author.

the main siamese network. Finally, we design a multi-level attention decoder to adaptively refine contextual information across different receptive fields, enabling precise localization and classification of changes.

To demonstrate its performance in real-world scenarios, we conducted experiments on two datasets. The first is the Gaza-change dataset, which we constructed and annotated for infrastructure damage assessment in the Gaza region. This dataset captures six categories of changes in civilian infrastructure between 2023 and 2024. The second is the classic SECOND dataset, whose labels were processed to retain only the changed areas, simulating an MCD task. Experimental results confirm that our model not only achieves leading performance but also possesses practical utility in complex real-world situations. Furthermore, Grad-CAM visualizations provide clear and interpretable evidence: the main path focuses on coarse-grained semantic context, while the auxiliary path concentrates on fine-grained structural details. This visual corroboration highlights the synergistic effect of the three-path design and explains the model’s ability to discern subtle change categories.

The main contributions of this paper are summarized as follows:

- 1) We propose Tri-path DINO, a novel complementary feature learning architecture that effectively adapts the pre-trained DINOv3 backbone for MCD by explicitly modeling complementary coarse-grained and fine-grained features.
- 2) We elucidate and validate the practical advantages of MCD over Binary Change Detection (BCD) and Semantic Change Detection (SCD) for tasks requiring annotation-efficient with empirical validation conducted on a damage assessment task.
- 3) We introduce the challenging Gaza-Change dataset for infrastructure damage assessment and demonstrate that our method achieves leading performance on both this dataset and the benchmark SECOND dataset.
- 4) We provide interpretable insights through visualization, revealing the independent yet complementary roles of the different feature paths within the architecture.

## II. RELATED WORK

Remote Sensing Change Detection (RSCD) aims to identify changes in the state of surface objects by analyzing images of the same geographical area acquired at different times. Depending on the task objectives, change detection can be mainly divided into three categories: Binary Change Detection (BCD), Multi-class Change Detection (MCD), and Semantic Change Detection (SCD). In recent years, with the advancement of deep learning, CD methods have achieved remarkable breakthroughs in performance. This section will review the research progress in these three categories and the CD methods based on pre-trained visual foundation models.

### A. Remote Sensing Change Detection

BCD aims to produce a binary mask that labels each pixel as “changed” or “unchanged.” Early approaches relied on traditional machine learning and image processing techniques [2].

With the deep learning revolution, siamese architectures based on convolutional neural networks have become mainstream. For example, the FC-Siam network [6], [7] employs weight-sharing to extract features from bi-temporal images. To enhance the feature extraction capability of convolutional networks, Fang et al. proposed SNUNet [8], which adopts dense skip connections in a U-shaped architecture. Furthermore, the inherently local receptive field of CNNs limits their ability to model long-range dependencies and capture global contextual information. To address this issue, researchers have introduced the attention mechanism and Transformer architecture [9], [10]. He et al. proposed a channel bias split attention (CBSA) to recover the information in the change region by adding a simple channel mapping [11]. The Transformer architecture establishes dynamic interactions among all elements within an image by utilizing a self-attention mechanism. This enables the model to explicitly model global dependencies and long-range contextual relationships, which is crucial for distinguishing genuine changes from spurious variations across different regions. In [12], a hybrid architecture combining Transformer and CNN, termed the BIT model, was proposed. This model employs a Transformer structure to process features obtained via convolution. In contrast, ChangeFormer [13] adopts a pure Transformer framework. Zhang et al. introduced Swin-SUNet [14], which incorporates the Swin Transformer [15] structure into the BCD task. These studies demonstrate the critical role of advanced network architecture design in feature extraction.

Both MCD [4] and SCD are inherently segmentation tasks, requiring higher-level semantic understanding compared to BCD. Due to the demand for fine-grained semantic annotations, most publicly available datasets are constructed under the BCD paradigm, resulting in relatively limited research and data resources dedicated to MCD and SCD. MCD aims to classify changed pixels into specific semantic categories. SCD, by nature, is a bi-temporal semantic segmentation task that requires generating precise semantic maps for each temporal phase. Owing to their fundamental similarities, the distinction between MCD and SCD is often not strictly emphasized in the literature [16]. Early research in SCD, such as [17], introduced an end-to-end recurrent convolutional neural network (ReCNN) that integrates the spectral-spatial feature extraction capabilities of CNNs with the temporal modeling strengths of RNNs. Long et al. proposed a multi-task learning framework that decomposes the detection of change regions into three sub-tasks: bi-temporal semantic segmentation, change detection, and boundary detection [18]. Ding et al. introduced SCanNet, which designs a semantic learning loss based on temporal consistency constraints [3]. Similarly, in [19], BCD is also incorporated as a subtask, and a contrastive learning module is designed to interact information between semantic detection and change detection.

### B. Visual Foundation Models

Visual Foundation Models (VFMs) acquire powerful general visual representation capabilities through pre-training on large-scale, multi-source datasets. This opens new perspectives for

visual change detection. CLIP [20] learns from image-text pairs to align visual and textual representations, enabling open-vocabulary reasoning. Segment Anything Model (SAM) [21] demonstrates exceptional zero-shot generalization capability on segmentation tasks. In contrast, the DINO series [5] relies solely on self-supervised learning to extract general-purpose visual features from massive datasets, making it well-suited as a feature encoder.

The success of VFMs has naturally attracted significant interest from researchers, and how to adapt and inject domain-specific knowledge into these foundation models has become a current focus. A common paradigm is to adopt SAM as the backbone, design it in a siamese architecture, and then train it on the target domain [22]. Furthermore, fine-tuning these VFMs has led to further performance improvements in change detection. For instance, [23] designed CNN adapters for this purpose. Meanwhile, [24] introduced a parameter-efficient fine-tuning approach using LoRA-like adapters. To mitigate the substantial parameter overhead of VFMs, [25] alternatively employed lightweight pre-trained variants such as FastSAM [26] and MobileSAM [27].

Despite the powerful representational capabilities of models like SAM, their robustness on remote sensing images remains limited, often struggling to identify RS-specific targets comprehensively. This significantly hinders the application of VFMs in SCD and MCD tasks. [28] first introduced SAM into the SCD task, meticulously designing a dual encoder-decoder architecture. This approach cross-fuses features from MobileSAM and a CNN encoder, and employs a multi-task scheme in the decoder to progressively decode features at different levels. [29] proposed a large-scale remote sensing dataset for fine-tuning and simultaneously utilized both CLIP and SAM to encode bi-temporal features. [30] was the first to incorporate DINO as a feature extractor for MCD, also adopting a multi-scale feature fusion architecture to enhance detection performance. In summary, effectively leveraging the potential of VFMs for high-level semantic tasks like SCD and MCD necessitates deliberate design of data and models.

### III. METHOD

In this section, we detail the design and training specifics of the proposed Tri-path DINO, covering the backbone siamese network architecture, the third-path siamese network structure, the decoder network architecture, and the composition of the loss function.

#### A. Overall

The overall architecture of the proposed Tri-path DINO is illustrated in Figure 1. It follows a siamese encoding and unified decoding paradigm, designed to extract and fuse complementary features from bi-temporal remote sensing images  $T_1$  and  $T_2$ . The framework consists of three cooperative parts, (1) the pre-trained DINOv3 backbone with CNN-based feature extractor, (2) Transformer feature extractor and (3) decoder.

#### B. DINO Backbone

Firstly, we introduce the backbone of Tri-path DINO. The backbone semantic encoder is built upon a pre-trained DINOv3. Given a pair of input images  $T_1$  and  $T_2$ , they are independently processed by the shared DINOv3 backbone, which terms as DINO siamese backbone. Subsequently, while keeping the original pre-trained weights frozen, we insert two types of lightweight adaptation modules, LoRA and adapter, into the backbone. As the primary feature extraction path, let the output features be denoted as  $S_1$  and  $S_2$ , respectively. Following this, a CNN feature extractor is appended. Denoting the output of the CNN feature extractor as  $f_{CNN}$ , we obtain:

$$f_{CNN} = FT_2([S_1 - S_2, FT_1([S_1, S_2])]), \quad (1)$$

where  $FT_1$  and  $FT_2$  are two convolutional feature processors, each consisting of a  $3 \times 3$  convolution followed by batch normalization, a GELU activation function, and a  $1 \times 1$  convolution.

Through multi-level extraction of the backbone features  $S_1$  and  $S_2$ , and by employing a carefully designed CNN feature extractor to process these features along with their difference feature, the backbone is guided to focus on local, coarse-grained targets.

#### C. The Third Path

To model long-range dependencies and capture fine-grained features between changing targets, we design a complementary context path at the bottom of Figure 1, also referred to as the third pathway. Let the intermediate features from the C2, C3, and C4 layers of the DINO backbone corresponding to the bi-temporal inputs  $T_1$  and  $T_2$  be denoted as  $[C_2, C_3, C_4]$  and  $[D_2, D_3, D_4]$ , respectively. Then we have:

$$Q = C_2 + D_2, \quad (2)$$

$$K = C_3 + D_3, \quad (3)$$

$$V = C_4 + D_4, \quad (4)$$

where  $Q, K$  and  $V$  are the input of the multi-head self-attention of the Transformer extractor. Then the Transformer feature  $f_{Tr}$  is obtained by

$$f_{Tr} = Attention(Q, K, V). \quad (5)$$

#### D. Enchanted Decoder

After completing the feature extraction from the two complementary paths, all features are fed into the decoder module located on the right side of Figure 1 for integration and refinement, ultimately generating a pixel-level multi-class change map. The core innovation of our decoder is the Multi-Level Hybrid Attention (MLHA), which adaptively fuses and enhances features from multi-scale and multi-semantic levels. Specifically, let the concatenated feature obtained from the CNN features and Transformer features be denoted as  $f_{fuse} = [f_{CNN}, f_{Tr}]$ . The MLHA module comprises two stages, initial fusion stage and final fusion stage. At the initial fusion stage, we process the concatenated features using parallel convolutional kernels (with kernel sizes of  $3 \times 3, 5 \times 5,$

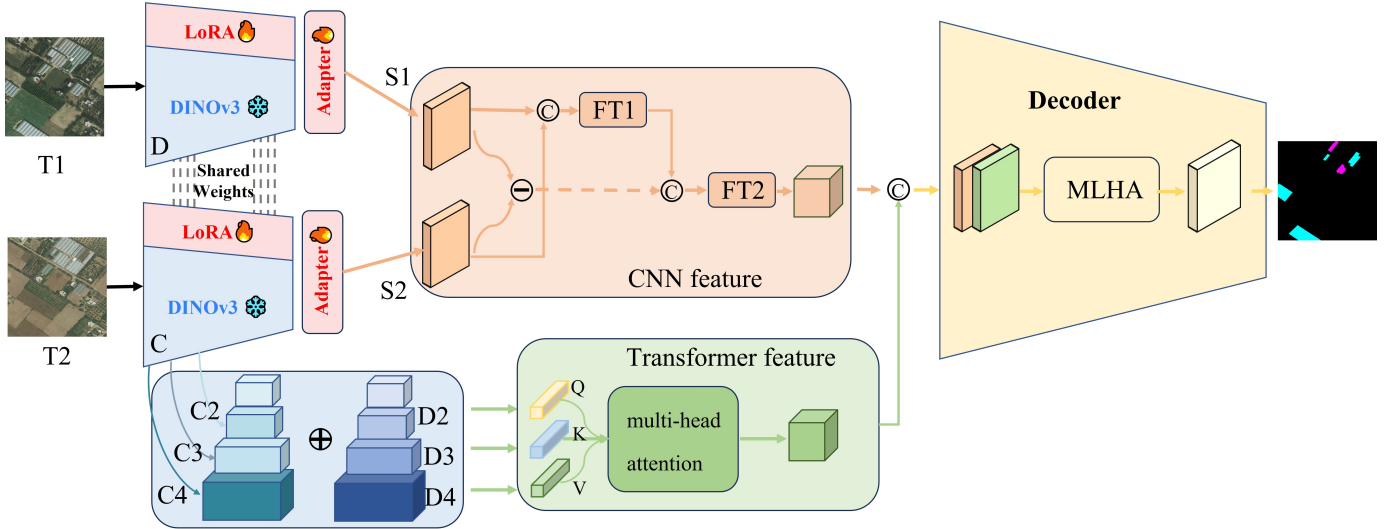


Fig. 1. Overall architecture of the proposed Tri-path DINO.

and  $7 \times 7$ ) to capture contextual patterns at different receptive fields. We have:

$$F_k = GELU(BN(Conv_k(X))), k = 1, 2, \dots, K, \quad (6)$$

$$F_{concat} = Concat(F_1, F_2, \dots, F_K) \quad (7)$$

$$X_{spatial} = f_{fuse} \odot \sigma(BN(Conv_{1 \times 1}(F_{concat}))), \quad (8)$$

$$y = f_{fuse} + GELU(BN(Conv_{3 \times 3}(X_{spatial}))). \quad (9)$$

At the final fusion stage, we employ three commonly used attention mechanisms to further extract distinct types of focused features, including channel attention, spatial attention, and local context. Then we have:

$$out = y + y_{channel} + y_{spatial} + y_{local}. \quad (10)$$

### E. Loss Function

In multi-class change detection for remote sensing imagery, the regions of interest (i.e., changed areas) typically occupy only a small fraction of the image. Moreover, severe class imbalance exists among different change categories. To mitigate these training challenges, various weighted loss functions have been proposed. In this work, we adopt a composite loss combining Focal Loss [31], Dice Loss [32], and Lovász Loss [33] to jointly address the class-imbalance issue. Focal Loss down-weights well-classified examples and focuses on hard samples; Dice Loss directly optimizes the overlap between predictions and ground truth; and Lovász Loss, as a differentiable surrogate for the Jaccard index, helps refine segmentation boundaries. The combination of these losses ensures stable gradient propagation and encourages the model to achieve balanced performance across all change categories. Then, we have:

$$\mathcal{L}_{total} = \alpha \mathcal{L}_{focal} + \beta \mathcal{L}_{Dice} + (1 - \alpha - \beta) \mathcal{L}_{LOVASZ}. \quad (11)$$

## IV. EXPERIMENTS

### A. Datasets

SECOND-CD [34] is a large-scale, high-quality dataset specifically constructed for semantic change detection. The imagery covers three major Chinese cities: Hangzhou, Chengdu, and Shanghai, comprising a total of 4,662 paired high-resolution aerial/satellite images with a size of  $512 \times 512$  pixels (spatial resolution 0.3–5 m). The dataset is split into 2,968 pairs for training and 1,694 pairs for testing. It provides bi-temporal semantic labels and change semantic labels, encompassing categories such as non-vegetated ground surface, tree, low vegetation, water, buildings, and playgrounds, along with their corresponding change information.

Gaza-change [30] is a dataset for multi-class change detection in the Gaza Strip. It comprises 922 precisely co-registered image pairs, each of  $512 \times 512$  pixels, captured by the Beijing-2 satellite (3.2 m Ground Sampling Distance) between 2023 and 2024. The imagery covers nine major urban areas, including Khan Yunis and Rafah. Following the annotation paradigm of MCD tasks, where only changes are annotated. The dataset labels the target pixel into one of six semantic change categories: building damage, new building, new camp, farmland damage, greenhouse damage, and new greenhouse. The dataset is randomly split into 554 pairs for training, 184 for validation, and 184 for testing.

### B. Implementation Details

All experiments in this paper were conducted on a single GPU (Nvidia RTX 3090 Ti) using the PyTorch framework. The models were trained for 150 epochs, with validation performed at the end of each epoch. We employed the AdamW optimizer with an initial learning rate of 0.0001 and a weight-decay coefficient of 0.05. The coefficients  $\alpha, \beta, \gamma$  in the loss function are set to 0.4, 0.3, and 0.3, respectively. Furthermore, to adapt the comparative methods to the MCD task, the output categories of these methods were correspondingly modified. It

should be noted that the SECOND dataset provides pixel-wise labels only for changed regions and does not supply separate bi-temporal semantic labels. We evaluated our method by comparing it with a range of state-of-the-art techniques that represent diverse methodological lines. The selected baselines include: BIT [12], SNUNet [35], LGPNet [36], ChangeFormer [13], USSFCNet [37], DDLNet [38], Rsmamba [39], CDxLstm [40], AnyChange [41], and MC-DiSNet [30].

### C. Evaluation Metrics

To comprehensively evaluate the performance of MCD tasks, we adopt the four metrics proposed in [42] (identical to those used for SCD): Overall Accuracy (OA), mean Intersection over Union (mIoU), Separated Kappa (SeK), and the SCD variant of the F1-score (denoted as  $F_{SCD}$ ). OA is defined as follows:

$$OA = \frac{\sum_{i=0}^N q_{ii}}{\sum_{i=0}^N \sum_{j=0}^N q_{ij}}, \quad (12)$$

where  $q_{ij}$  denotes an element of the confusion matrix, representing the number of pixels whose ground-truth class is  $j$  but are predicted as class  $i$ . Here, class 0 corresponds to the background (no change). OA measures the proportion of all pixels that are correctly classified.

In both SCD and MCD tasks, the mean Intersection over Union (mIoU) focuses exclusively on the "changed" categories. Its formula is given as follows:

$$mIoU = \frac{IoU_{nc} + IoU_c}{2}, \quad (13)$$

$$IoU_{nc} = \frac{q_{00}}{\sum_{i=1}^N q_{i0} + \sum_{j=1}^N q_{0j} - q_{00}}, \quad (14)$$

$$IoU_c = \frac{\sum_{i=1}^N \sum_{j=1}^N q_{ij}}{\sum_{i=0}^N \sum_{j=0}^N q_{ij} - q_{00}}. \quad (15)$$

The SeK coefficient specifically assesses the model's performance on the critical task of identifying "changed" regions. Let  $\hat{q}_{ij} = q_{ij}$  except for entries corresponding to the "no-change" (background) class. Then the formula is:

$$\rho = \frac{\sum_{i=1}^N \hat{q}_{ii}}{\sum_{i=0}^N \sum_{j=0}^N \hat{q}_{ij}}, \quad (16)$$

$$\eta = \frac{\sum_{i=0}^N (\sum_{j=0}^N \hat{q}_{ij} \cdot \sum_{j=0}^N \hat{q}_{ji})}{(\sum_{i=0}^N \sum_{j=0}^N \hat{q}_{ij})^2}, \quad (17)$$

$$Sek = e^{IoU_c - 1} \cdot \frac{(\rho - \eta)}{(1 - \eta)}. \quad (18)$$

Similarly,  $F_{scd}$  is computed exclusively within regions annotated as "changed." The metric first calculates precision and recall considering only the changed-class pixels, and then derives their harmonic mean as follows:

$$P_{scd} = \frac{\sum_{i=1}^N q_{ii}}{\sum_{i=1}^N \sum_{j=0}^N q_{ij}}, \quad (19)$$

$$R_{scd} = \frac{\sum_{i=1}^N q_{ii}}{\sum_{i=0}^N \sum_{j=1}^N q_{ij}}, \quad (20)$$

$$F_{scd} = \frac{2 \cdot P_{scd} \cdot R_{scd}}{P_{scd} + R_{scd}}. \quad (21)$$

### D. Main Results

As shown in Figure 2 and Figure 3, we present a visual comparison of the detection results of different methods on the Gaza-change dataset. Tri-path DINO produces clearer detection boundaries, indicating that the proposed complementary learning architecture enables the model to better understand the detailed features of changes. Meanwhile, by observing the results in the first row of Figure 2 and the second row of Figure 3, it can be seen that the proposed method improves the recognition rate of small targets and avoids the false detections encountered by other methods, demonstrating the high detection performance of Tri-path DINO for fine-grained features. For larger targets, Tri-path achieves the most complete detection. This ability to adapt to targets of varying sizes strongly demonstrates the potential of the complementary learning framework in remote sensing tasks.

Compared with the facility damage, the SECOND dataset contains more detailed variations. Figure 4 and Figure 5 present the detection results of various state-of-the-art methods on this dataset. It can be clearly observed that the proposed Tri-path DINO captures finer details. In particular, the gaps between buildings in the third row are identified, a capability not achieved by other methods. Additionally, the subtle changes in the central area of the fourth row are also recognized, reflecting the sensitivity of complementary learning to changes. In summary, the complementary learning framework significantly enhances the discriminative ability of the pre-trained model for fine-grained features.

As reported in Table I, our proposed Tri-path DINO achieves the best performance across all four evaluation metrics. Specifically, our model attains an OA of 96.45% and an mIoU of 71.35%, representing improvements of 0.12% and 0.71%, respectively, over the previous best method, MC-DiSNet. This validates the superiority of our model in terms of overall classification accuracy and segmentation consistency across various change categories. More importantly, on the Sek and  $F_{scd}$  metrics, which better reflect a model's ability to distinguish between imbalanced change classes, our method achieves significant leads of 13.02 and 62.58, substantially outperforming all other compared methods.

We compared various methods on the classic SECOND dataset. Table II shows that Tri-path DINO achieves highly competitive performance on this standard benchmark. Notably, our method attains the highest scores in three key metrics: mIoU (71.62%), Sek (20.61), and  $F_{scd}$  (55.44). Compared to the previous state-of-the-art method, MC-DiSNet, Tri-path DINO outperforms it across all four evaluated metrics, demonstrating the effectiveness of the complementary feature learning strategy. In contrast, the AnyChange method, based on a pre-trained foundational model, performs significantly below expectations due to its difficulty in handling shifts in

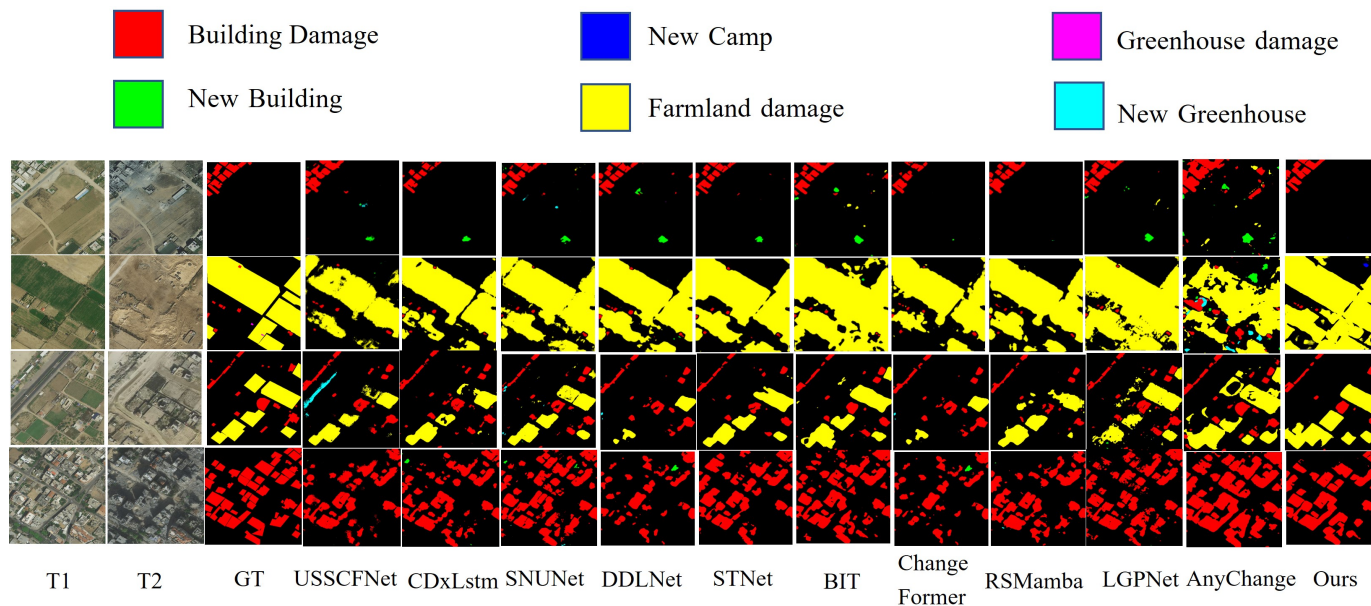


Fig. 2. Example results on Gaza-change dataset.

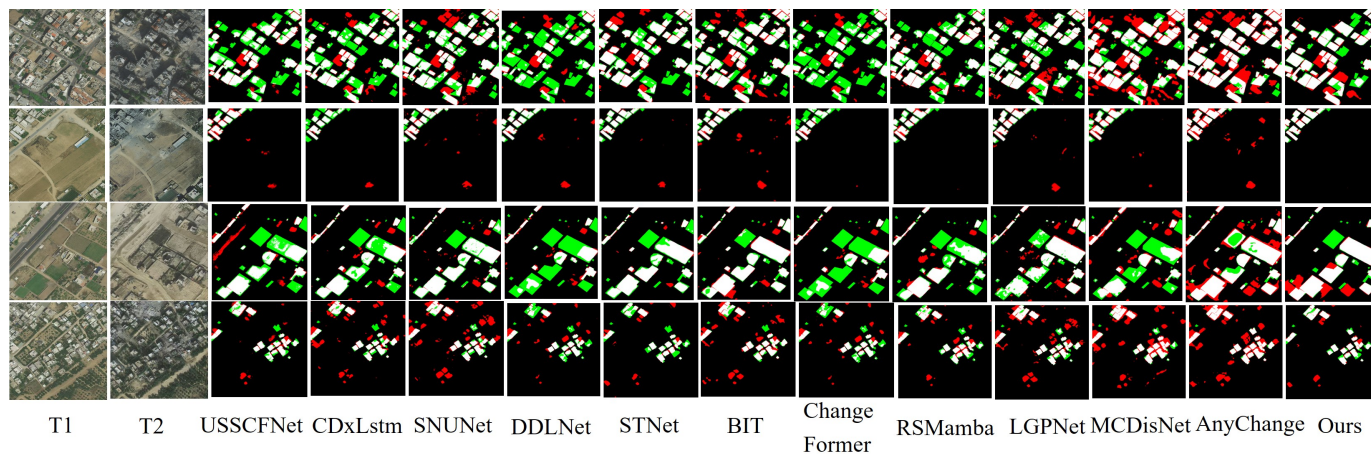


Fig. 3. Qualitative comparison on the Gaza-Change dataset, with color coding: true positives (white), true negatives (black), false positives (red), and false negatives (green).

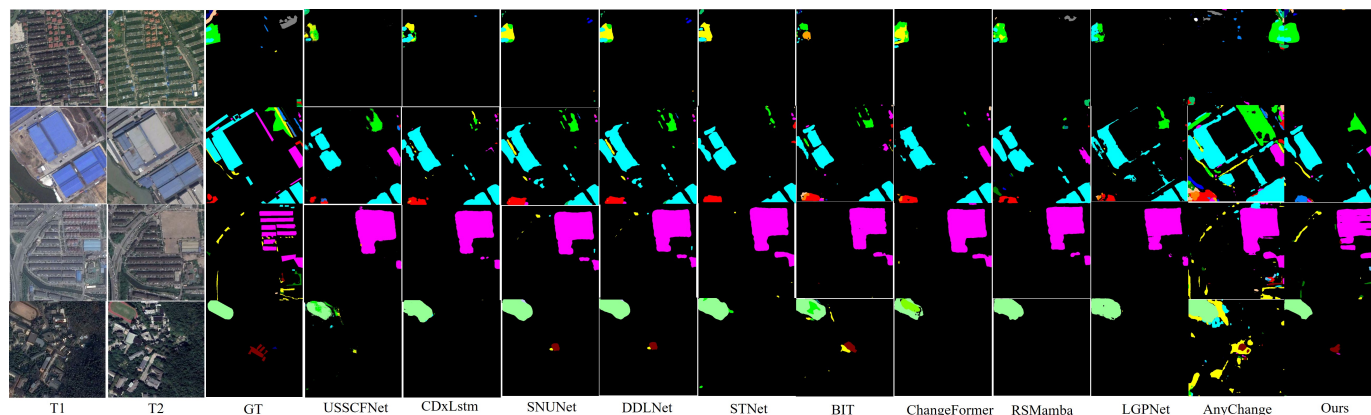


Fig. 4. Example results on SECOND dataset.

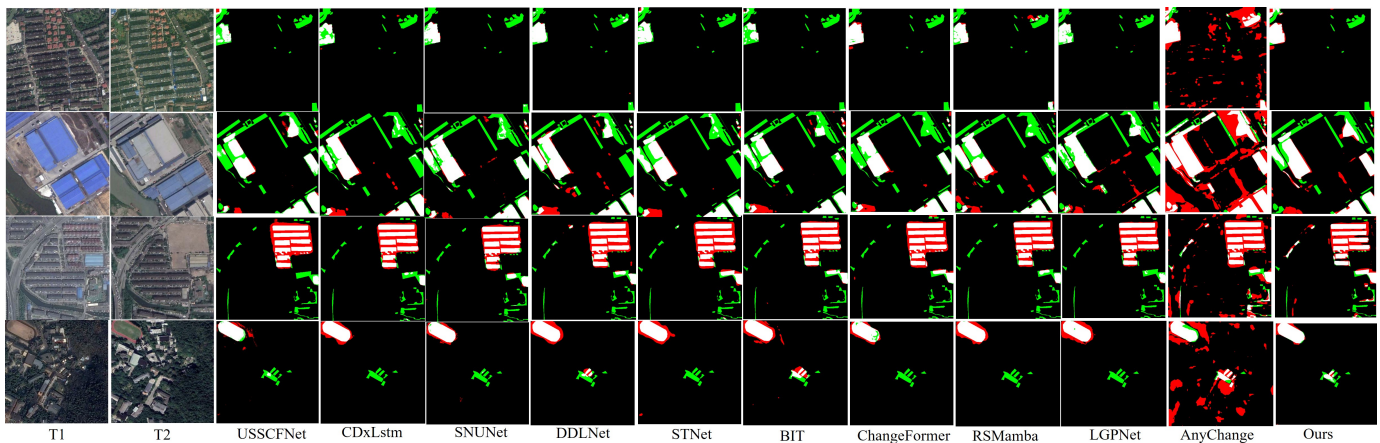


Fig. 5. Qualitative comparison on the SECOND dataset, with color coding: true positives (white), true negatives (black), false positives (red), and false negatives (green).

Methods	OA	mIoU	Sek	$F_{scd}$
BIT	95.74	68.81	8.91	57.85
CDxLstm	96.06	67.97	7.3	55.36
ChangeFormer	95.92	66.48	5.29	52.64
DDLNet	96.28	69.39	10.28	58.87
LGPNet	95.49	68.24	9.16	56.97
Rsmamba	96.22	67.53	7.26	54.89
SNUNet	95.53	67.75	7.26	55.58
STNet	96.20	69.69	10.21	59.49
USSFCNet	95.90	66.25	5.70	51.57
MC-DiSNet	96.33	70.64	11.73	60.8
AnyChange	93.70	64.48	5.27	50.42
<b>Ours</b>	<b>96.45</b>	<b>71.35</b>	<b>13.02</b>	<b>62.58</b>

TABLE I

COMPREHENSIVE COMPARISON WITH STATE-OF-THE-ART METHODS ON THE GAZA-CHANGE DATASET.

Methods	OA	mIoU	Sek	$F_{scd}$
BIT	86.77	70.79	19.28	54.52
CDxLstm	86.29	70.38	17.89	52.58
ChangeFormer	86.36	70.26	18.35	53.55
DDLNet	86.47	71.12	19.06	53.78
LGPNet	86.57	69.67	17.49	53.05
Rsmamba	86.51	69.64	17.63	52.71
SNUNet	85.82	68.61	15.29	49.69
STNet	86.65	68.61	18.84	53.65
USSFCNet	85.52	68.7	14.93	49.45
MC-DiSNet	85.97	71.14	19.75	53.91
AnyChange	65.84	51.94	9.37	36.61
<b>Ours</b>	<b>86.33</b>	<b>71.62</b>	<b>20.61</b>	<b>55.44</b>

TABLE II

COMPREHENSIVE COMPARISON WITH STATE-OF-THE-ART METHODS ON THE SECOND DATASET.

input distribution, highlighting the necessity of our fine-tuning strategy.

### E. Ablation Study

We conducted systematic ablation experiments on the Gaza-change and SECOND datasets to validate the effectiveness of the proposed third path and the MLHA module. The experimental results are shown in Table III and Table IV, where Path indicates whether the third path is introduced, and MLHA indicates whether the Multi-Level Hybrid Attention

module is used in the decoder. Evidently, the performance when using either the MLHA module alone or introducing the third path (Path) alone is significantly better than the baseline, where neither module is used. This demonstrates the important contribution of both multi-level attention fusion and fine-grained complementary feature modeling to improving MCD performance. When both Path and MLHA are enabled (i.e., the complete Tri-path DINO), the model achieves the best performance across all key metrics on both datasets. This indicates a significant synergistic and complementary relationship between the encoder and decoder module designs.

TABLE III

MODULE-LEVEL ABLATION RESULTS ON THE GAZA-CHANGE DATASET. BEST SCORES ARE IN BOLD.

Path	MLHA	OA	mIoU	Sek	$F_{scd}$
		95.63	69.66	11.79	59.42
	✓	96.33	70.64	11.73	60.8
✓	✓	<b>96.45</b>	<b>71.35</b>	<b>13.02</b>	<b>62.58</b>

TABLE IV

MODULE-LEVEL ABLATION RESULTS ON THE SECOND DATASET. BEST SCORES ARE IN BOLD.

Path	MLHA	OA	mIoU	Sek	$F_{scd}$
		85.46	70.22	18.6	53.26
	✓	85.97	71.14	19.7	53.91
✓	✓	<b>86.33</b>	<b>71.62</b>	<b>20.61</b>	<b>55.44</b>

### F. Grad-CAM Visualization

To intuitively validate the complementary roles of each path in Tri-path DINO and elucidate the model’s decision-making mechanism, we employ the Grad-CAM method to visualize its regions of focus. As shown in Figure 6, the primary backbone path predominantly activates coarse-grained semantic regions (such as entire building areas). In contrast, the features from the third pathway concentrate on local, previously unattended areas. This clear functional division demonstrates that the two paths inherently capture complementary information: the

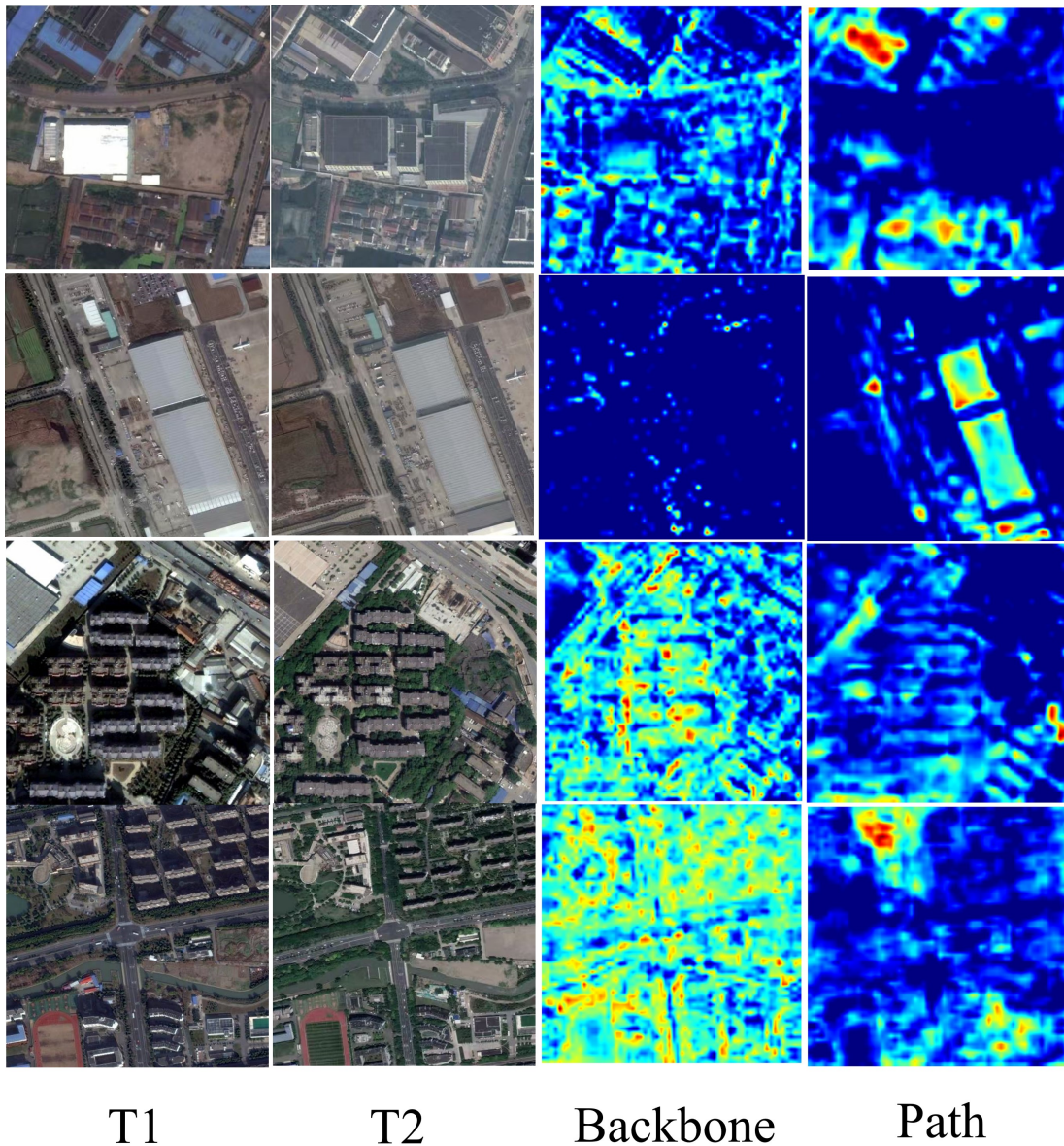


Fig. 6. Heatmaps based on the GradCAM visualization, Path represents the features learned by the third pathway, while Backbone represents the features learned by the backbone siamese network.

primary path provides high-level semantic localization, while the third path supplies detailed contextual evidence.

## V. CONCLUSION

This paper proposes a novel network architecture for multi-class change detection in high-resolution remote sensing imagery, which can be efficiently applied to remote sensing monitoring scenarios. To address the challenges of MCD, where target regions are extremely small and inter-class feature differences are subtle, we designed a context-complementary feature learning architecture, utilizing a pre-trained DINOv3 model as the feature extractor. The backbone network employs a CNN for feature extraction to enhance the learning of coarse-grained features. Intermediate multi-layer features are fed into

a Transformer feature extractor to achieve fine-grained feature learning. A Multi-Level Hybrid Attention (MLHA) module is incorporated into the decoder to improve adaptive multi-scale feature refinement. Extensive experiments on the real-world challenging Gaza-change damage assessment dataset and the standard SECOND benchmark demonstrate the effectiveness of the proposed method. Our work confirms that the MCD framework offers a practical and annotation-efficient balance between binary change detection and full semantic change detection, especially suitable for time-sensitive, fine-grained applications such as post-disaster damage assessment. Although Tri-path DINO has shown strong performance, future work may extend it to multi-temporal change analysis and

explore more efficient designs for real-time processing.

## REFERENCES

- [1] L. Ding, D. Hong, M. Zhao, H. Chen, C. Li, J. Deng, N. Yokoya, L. Bruzzone, J. Chanussot, A survey of sample-efficient deep learning for change detection in remote sensing: Tasks, strategies, and challenges, *IEEE Geoscience and Remote Sensing Magazine* 13 (3) (2025) 164–189. doi:10.1109/MGRS.2025.3533605.
- [2] S. Marchesi, L. Bruzzone, Ica and kernel ica for change detection in multispectral remote sensing images, in: 2009 IEEE International Geoscience and Remote Sensing Symposium, Vol. 2, IEEE, 2009, pp. II–980.
- [3] L. Ding, J. Zhang, H. Guo, K. Zhang, B. Liu, L. Bruzzone, Joint spatio-temporal modeling for semantic change detection in remote sensing images, *IEEE Transactions on Geoscience and Remote Sensing* 62 (2024) 1–14.
- [4] Q. Zhu, X. Guo, Z. Li, D. Li, A review of multi-class change detection for satellite remote sensing imagery, *Geo-spatial Information Science* 27 (1) (2024) 1–15.
- [5] O. Siméoni, H. V. Vo, M. Seitzer, F. Baldassarre, M. Oquab, C. Jose, V. Khalidov, M. Szafraniec, S. Yi, M. Ramamonjisoa, et al., Dinov3, arXiv preprint arXiv:2508.10104 (2025).
- [6] R. C. Daudt, B. Le Saux, A. Boulch, Fully convolutional siamese networks for change detection, in: 2018 25th IEEE international conference on image processing (ICIP), IEEE, 2018, pp. 4063–4067.
- [7] Y. Zhan, K. Fu, M. Yan, X. Sun, H. Wang, X. Qiu, Change detection based on deep siamese convolutional network for optical aerial images, *IEEE Geoscience and Remote Sensing Letters* 14 (10) (2017) 1845–1849.
- [8] S. Fang, K. Li, J. Shao, Z. Li, Snunet-cd: A densely connected siamese network for change detection of vhr images, *IEEE Geoscience and Remote Sensing Letters* 19 (2021) 1–5.
- [9] A. Vaswani, N. Shazeer, N. Parmar, J. Uszkoreit, L. Jones, A. N. Gomez, L. Kaiser, I. Polosukhin, Attention is all you need, *Advances in neural information processing systems* 30 (2017).
- [10] A. Dosovitskiy, L. Beyer, A. Kolesnikov, D. Weissenborn, X. Zhai, T. Unterthiner, M. Dehghani, M. Minderer, G. Heigold, S. Gelly, J. Uszkoreit, N. Houlsby, An image is worth 16x16 words: Transformers for image recognition at scale, *ICLR* (2021).
- [11] N. He, L. Wang, P. Zheng, C. Zhang, L. Li, Cbsasnet: A siamese network based on channel bias split attention for remote sensing change detection, *IEEE Transactions on Geoscience and Remote Sensing* 62 (2024) 1–17.
- [12] H. Chen, Z. Qi, Z. Shi, Remote sensing image change detection with transformers, *IEEE Transactions on Geoscience and Remote Sensing* 60 (2021) 1–14.
- [13] W. G. C. Bandara, V. M. Patel, A transformer-based siamese network for change detection, in: IGARSS 2022-2022 IEEE International Geoscience and Remote Sensing Symposium, IEEE, 2022, pp. 207–210.
- [14] C. Zhang, L. Wang, S. Cheng, Y. Li, Swinsunet: Pure transformer network for remote sensing image change detection, *IEEE Transactions on Geoscience and Remote Sensing* 60 (2022) 1–13.
- [15] Z. Liu, Y. Lin, Y. Cao, H. Hu, Y. Wei, Z. Zhang, S. Lin, B. Guo, Swin transformer: Hierarchical vision transformer using shifted windows, in: Proceedings of the IEEE/CVF international conference on computer vision, 2021, pp. 10012–10022.
- [16] F. Cui, J. Jiang, Mtsd-net: A network based on multi-task learning for semantic change detection of bitemporal remote sensing images, *International Journal of Applied Earth Observation and Geoinformation* 118 (2023) 103294.
- [17] L. Mou, L. Bruzzone, X. X. Zhu, Learning spectral-spatial-temporal features via a recurrent convolutional neural network for change detection in multispectral imagery, *IEEE Transactions on Geoscience and Remote Sensing* 57 (2) (2018) 924–935.
- [18] J. Long, S. Liu, M. Li, H. Zhao, Y. Jin, Bgsnet: A boundary-guided siamese multitask network for semantic change detection from high-resolution remote sensing images, *ISPRS Journal of Photogrammetry and Remote Sensing* 225 (2025) 221–237.
- [19] K. Tang, F. Xu, X. Chen, Q. Dong, Y. Yuan, J. Chen, The clearscd model: Comprehensively leveraging semantics and change relationships for semantic change detection in high spatial resolution remote sensing imagery, *ISPRS Journal of Photogrammetry and Remote Sensing* 211 (2024) 299–317. doi:https://doi.org/10.1016/j.isprsjprs.2024.04.013. URL https://www.sciencedirect.com/science/article/pii/S0924271624001734
- [20] A. Radford, J. W. Kim, C. Hallacy, A. Ramesh, G. Goh, S. Agarwal, G. Sastry, A. Askell, P. Mishkin, J. Clark, et al., Learning transferable visual models from natural language supervision, in: International conference on machine learning, Pmlr, 2021, pp. 8748–8763.
- [21] A. Kirillov, E. Mintun, N. Ravi, H. Mao, C. Rolland, L. Gustafson, T. Xiao, S. Whitehead, A. C. Berg, W.-Y. Lo, et al., Segment anything, in: Proceedings of the IEEE/CVF international conference on computer vision, 2023, pp. 4015–4026.
- [22] Y. Qin, C. Wang, Y. Fan, C. Pan, Sam2-cd: Remote sensing image change detection with sam2, *IEEE Journal of Selected Topics in Applied Earth Observations and Remote Sensing* (2025).
- [23] J. Gao, D. Zhang, F. Wang, L. Ning, Z. Zhao, X. Li, Combining sam with limited data for change detection in remote sensing, *IEEE Transactions on Geoscience and Remote Sensing* (2025).
- [24] D. Zhang, F. Wang, L. Ning, Z. Zhao, J. Gao, X. Li, Integrating sam with feature interaction for remote sensing change detection, *IEEE Transactions on Geoscience and Remote Sensing* (2024).
- [25] L. Ding, K. Zhu, D. Peng, H. Tang, K. Yang, L. Bruzzone, Adapting segment anything model for change detection in vhr remote sensing images, *IEEE Transactions on Geoscience and Remote Sensing* 62 (2024) 1–11.
- [26] X. Zhao, W. Ding, Y. An, Y. Du, T. Yu, M. Li, M. Tang, J. Wang, Fast segment anything, arXiv preprint arXiv:2306.12156 (2023).
- [27] C. Zhang, D. Han, Y. Qiao, J. U. Kim, S.-H. Bae, S. Lee, C. S. Hong, Faster segment anything: Towards lightweight sam for mobile applications, arXiv preprint arXiv:2306.14289 (2023).
- [28] L. Mei, Z. Ye, C. Xu, H. Wang, Y. Wang, C. Lei, W. Yang, Y. Li, Scd-sam: Adapting segment anything model for semantic change detection in remote sensing imagery, *IEEE Transactions on Geoscience and Remote Sensing* 62 (2024) 1–13.
- [29] W. Jiang, Y. Sun, L. Lei, G. Kuang, K. Ji, Adaptvfms-rscd: Advancing remote sensing change detection from binary to semantic with sam and clip, *ISPRS Journal of Photogrammetry and Remote Sensing* 230 (2025) 304–317.
- [30] K. Zheng, Z. Wu, F. Wei, M. Zhou, K. Lie, H. Guo, L. Ding, W. Zhang, H.-C. Dong, Changes in gaza: Dinov3-powered multi-class change detection for damage assessment in conflict zones, arXiv preprint arXiv:2511.19035v2 (2025).
- [31] T.-Y. Lin, P. Goyal, R. Girshick, K. He, P. Dollár, Focal loss for dense object detection, in: Proceedings of the IEEE international conference on computer vision, 2017, pp. 2980–2988.
- [32] F. Milletari, N. Navab, S.-A. Ahmadi, V-net: Fully convolutional neural networks for volumetric medical image segmentation, in: 2016 fourth international conference on 3D vision (3DV), Ieee, 2016, pp. 565–571.
- [33] M. Berman, A. R. Triki, M. B. Blaschko, The lovász-softmax loss: A tractable surrogate for the optimization of the intersection-over-union measure in neural networks, in: Proceedings of the IEEE conference on computer vision and pattern recognition, 2018, pp. 4413–4421.
- [34] K. Yang, G.-S. Xia, Z. Liu, B. Du, W. Yang, M. Pelillo, L. Zhang, Asymmetric siamese networks for semantic change detection in aerial images, *IEEE Transactions on Geoscience and Remote Sensing* 60 (2021) 1–18.
- [35] S. Fang, K. Li, J. Shao, Z. Li, Snunet-cd: A densely connected siamese network for change detection of vhr images, *IEEE Geoscience and Remote Sensing Letters* 19 (2021) 1–5.
- [36] T. Liu, M. Gong, D. Lu, Q. Zhang, H. Zheng, F. Jiang, M. Zhang, Building change detection for vhr remote sensing images via local-global pyramid network and cross-task transfer learning strategy, *IEEE Transactions on Geoscience and Remote Sensing* 60 (2021) 1–17.
- [37] T. Lei, X. Geng, H. Ning, Z. Lv, M. Gong, Y. Jin, A. K. Nandi, Ultralightweight spatial-spectral feature cooperation network for change detection in remote sensing images, *IEEE Transactions on Geoscience and Remote Sensing* 61 (2023) 1–14. doi:10.1109/TGRS.2023.3261273.
- [38] X. Ma, J. Yang, R. Che, H. Zhang, W. Zhang, Ddlnet: Boosting remote sensing change detection with dual-domain learning, in: 2024 IEEE International Conference on Multimedia and Expo (ICME), IEEE, 2024, pp. 1–6.
- [39] C. Liu, K. Chen, B. Chen, H. Zhang, Z. Zou, Z. Shi, Rscama: Remote sensing image change captioning with state space model, *IEEE Geoscience and Remote Sensing Letters* 21 (2024) 1–5.
- [40] Z. Wu, X. Ma, R. Lian, K. Zheng, W. Zhang, Cdxlstm: Boosting remote sensing change detection with extended long short-term memory, *IEEE Geoscience and Remote Sensing Letters* (2025).
- [41] Z. Zheng, Y. Zhong, L. Zhang, S. Ermon, Segment any change, in: A. Globerson, L. Mackey, D. Belgrave, A. Fan, U. Paquet, J. Tomczak, C. Zhang (Eds.), *Advances in Neural Information*

Processing Systems, Vol. 37, Curran Associates, Inc., 2024, pp. 81204–81224. doi:10.52202/079017-2581.

URL [https://proceedings.neurips.cc/paper\\_files/paper/2024/file/9415416201aa201902d1743c7e65787b-Paper-Conference.pdf](https://proceedings.neurips.cc/paper_files/paper/2024/file/9415416201aa201902d1743c7e65787b-Paper-Conference.pdf)

- [42] L. Ding, H. Guo, S. Liu, L. Mou, J. Zhang, L. Bruzzone, Bi-temporal semantic reasoning for the semantic change detection in hr remote sensing images, IEEE Transactions on Geoscience and Remote Sensing 60 (2022) 1–14.